OPEN ACCESS

Journal of Science & Cycling
Breakthroughs in Cycling & Triathlon Sciences

Original Article

BMX Race-Start Dynamics: Coupling On-Track Measurements and Physics-Based Modelling for Performance Optimisation

Antonin Fortier [1], Mickaël Violain [2], Emmanuel Brunet [2] and Christophe Clanet [1,*]

Received: 26 July 2025 **Accepted:** 12 November 2025 **Published:** 8 December 2025

[1] LadHyX, CNRS–Ecole Polytechnique, Institut Polytechnique de Paris, 91120 Palaiseau, France´

[2] Fédération Française de Cyclisme, 1 rue Laurent Fignon, 78390 Montigny-le-Bretonneux, France

Correspondence

Christophe Clanet

LadHyX, CNRS–Ecole Polytechnique, Institut Polytechnique de Paris, 91120 Palaiseau, France´

christophe.clanet@polytechnique.edu

Abstract

A fast and stable launch is decisive in Bicycle Moto-Cross (BMX) racing, yet the underlying interplay between rider power production, bicycle gearing and ramp geometry has received little attention in the engineering literature. Using high-frequency field measurements gathered on the Olympic track of Saint Quentin-en-Yvelines (France), we develop and validate a physics-based model that predicts the rider's velocity profile over the start ramp. The formulation combines (i) a Hill-type linear torque–cadence relationship fitted to instrumented-crank data, (ii) an energy balance that accounts for aerodynamic and rolling losses, and (iii) the measured track slope. Model predictions agree with experiments for three gear ratios. We then explore two practical optimisation criteria—minimum time to the first bump and maximum mean acceleration on the ramp—to identify gearing strategies tailored to individual athletes. The framework illustrates how on-track sensing can be translated into actionable engineering guidelines for coaches and riders.

Keywords

BMX Racing; Start Mechanics; Gear Ratio; Instrumented Crank; Optimisation

1 Introduction

Bicycle Moto-Cross (BMX) emerged in the United States during the early 1970s [1, 2]. The creation of the International BMX Federation in 1981 and the first World Championships a year later paved the way for full integration into the Union Cycliste Internationale (UCI) in 1993 [3]. Since Beijing 2008, BMX racing has featured on the Olympic programme; BMX freestyle followed in Tokyo 2021 [4]. Compared with road bicycles, BMX machines exhibit markedly

different geometries and, crucially, a single–speed drivetrain with no possibility of shifting on course [5]. The gear ratio $G = R_1/R_2$ (figure 1b) therefore becomes a strategic parameter that riders must choose in advance, balancing their individual torque–cadence capabilities against track characteristics [6, 7, 8, 9].

In Olympic-class racing, eight riders sprint down an 8m-high start ramp (figure 1a) onto a 400m track comprising four technical straights linked by banked turns (figure 2). Elite races last roughly 40s [10, 11] and thus fall into the domain of maximal-intensity sprint cycling [12]. Previous work in sprint sports—speed skating [13] or short-distance athletics [14]—has shown that early-phase performance strongly conditions final ranking. For BMX racing, Rylands [15] demonstrated that the first 8–10s of the run are highly predictive of finishing position, regardless of gender or track design, a finding echoed by subsequent studies [16, 17, 18]. Securing the lead at the first jump allows a rider to dictate line choice into the opening corner [19, 20, 21], motivating coaches to devote substantial training time to start technique [22, 23].

Despite this competitive importance, few models couple the mechanical constraints of a fixed-gear bicycle with the non-trivial topography of modern BMX ramps. The present study aims to fill that gap. Using rider-specific field data recorded on the Olympic track of Saint-Quentin-en-Yvelines, we (i) establish a dynamically consistent model for the start phase and (ii) employ it to determine, for a given athlete and strategy, the gear ratio that maximises a chosen performance criterion. The remainder of the paper is organised as follows. Section 2 details the measurement campaign and sensor set-up; Section 3 reports key experimental findings. A physics-based model is then formulated (Section 4) and validated against the data, after which optimisation scenarios are explored in section 5. Conclusions and perspectives close the paper.

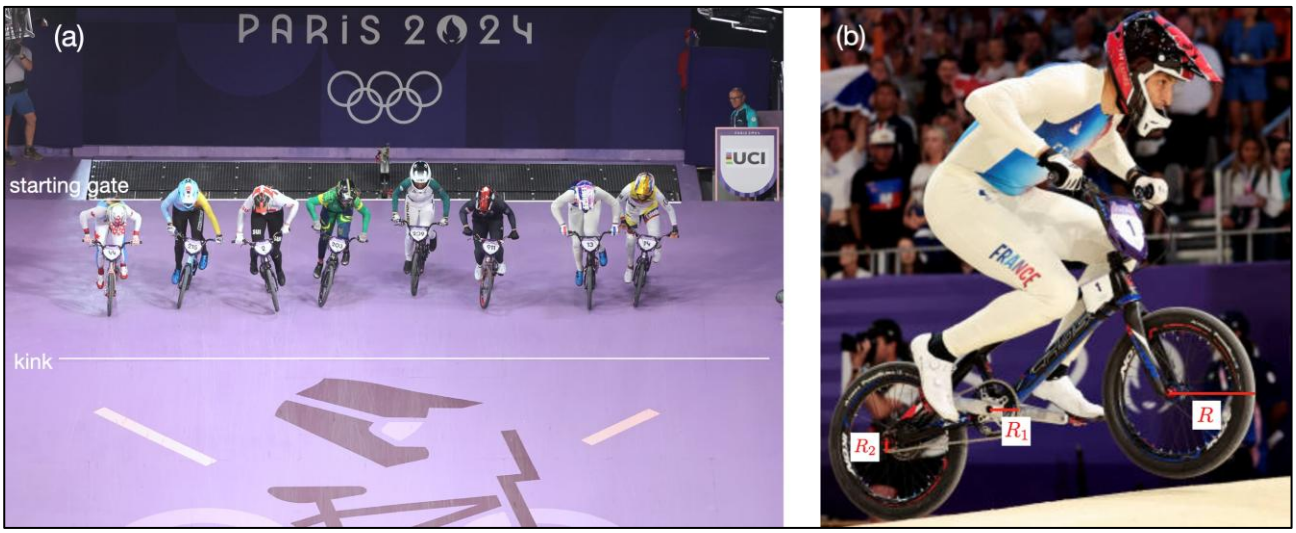

Figure 1. (a) Eight riders just after the standing start in a BMX race, between the starting grid and the *kink*. (b) BMX rider and bicycle illustrating the fixed gear ratio $G = R_1/R_2$, where R_1 and R_2 denote the radii of the chainring and rear sprocket, respectively; R is the wheel radius.
Photo © Patrick Pichon – Fédération Française de Cyclisme.

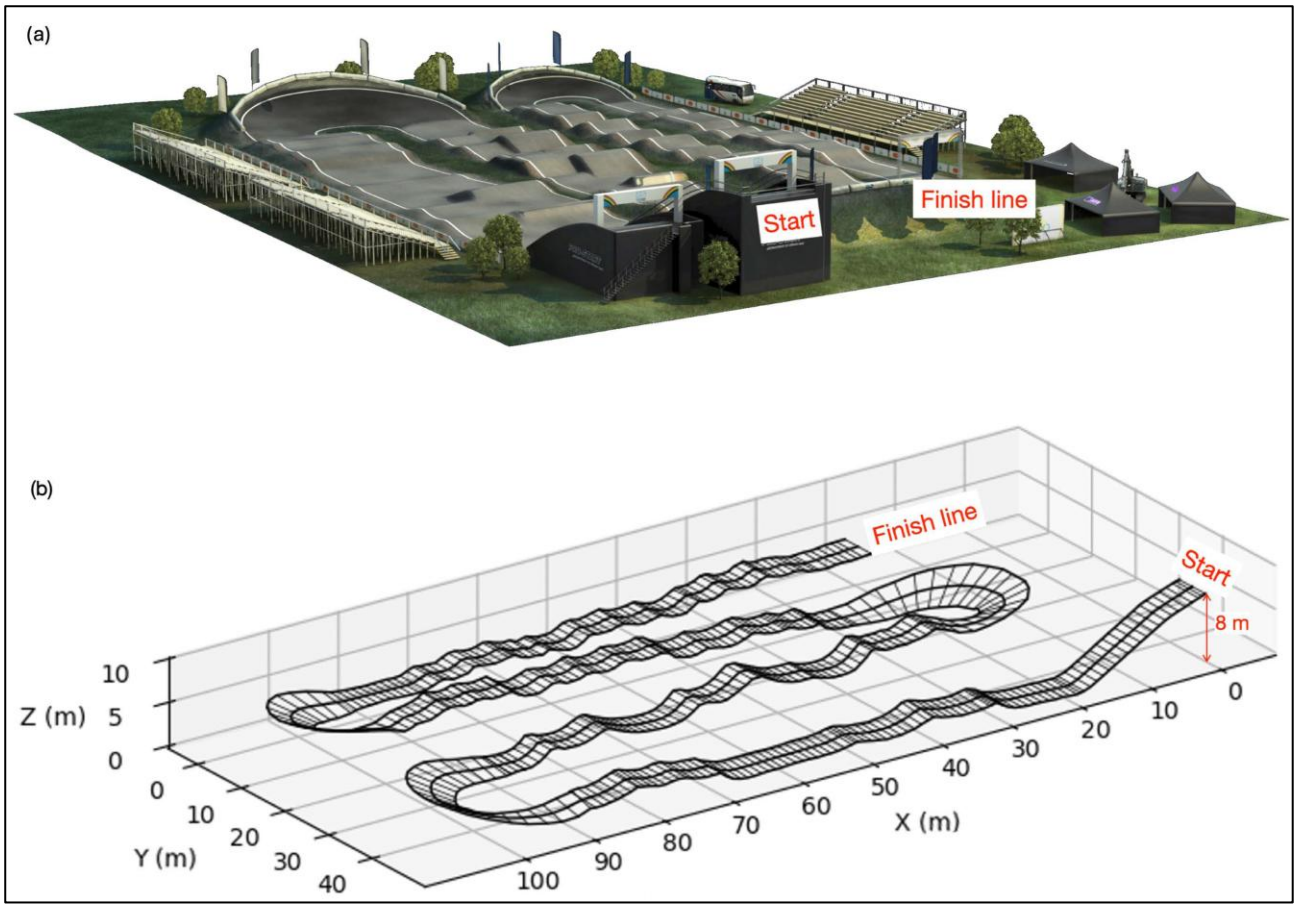

Figure 2. 3-D views of SQY BMX Stadium: (a) designer's rendering; (b) reconstructed centre-line profile of the elite track derived from inclinometer measurements.

2 Experimental Conditions

2.1 Topography of the BMX Track

All measurements were carried out at the BMX Stadium of Saint-Quentin-en-Yvelines (SQY), the venue used for the Paris 2024 Olympic Games.

2.1.1 Full BMX Track

The elite track, designed by Protracks, features an 8m-high start ramp and a total length of 400m. A detailed survey was performed with a digital inclinometer at 1m longitudinal intervals and at the crest of each bump. Figure 2a shows the architect's 3-D rendering, while Figure 2b presents the reconstructed centre-line profile obtained from the survey.

2.1.2 The "Start Ramp"

During a race, eight riders launch simultaneously from the top platform (figure 1a and Zone 0 in figure 3). Standard Olympic geometry prescribes an initial ramp slope of 18° for the first 5m (Zone 1), steepening to 28° (Zone 2) until the curved transition (Zone 3). The flat lead-in to the first bump (Zone 4) is 6m long, followed by the bump itself (Zone 5). Figure 3 details these regions and the local slope $\alpha(s)$. See the UCI BMX Track Guide and Part VI of the UCI Cycling Regulations for exact specifications [3, 24].

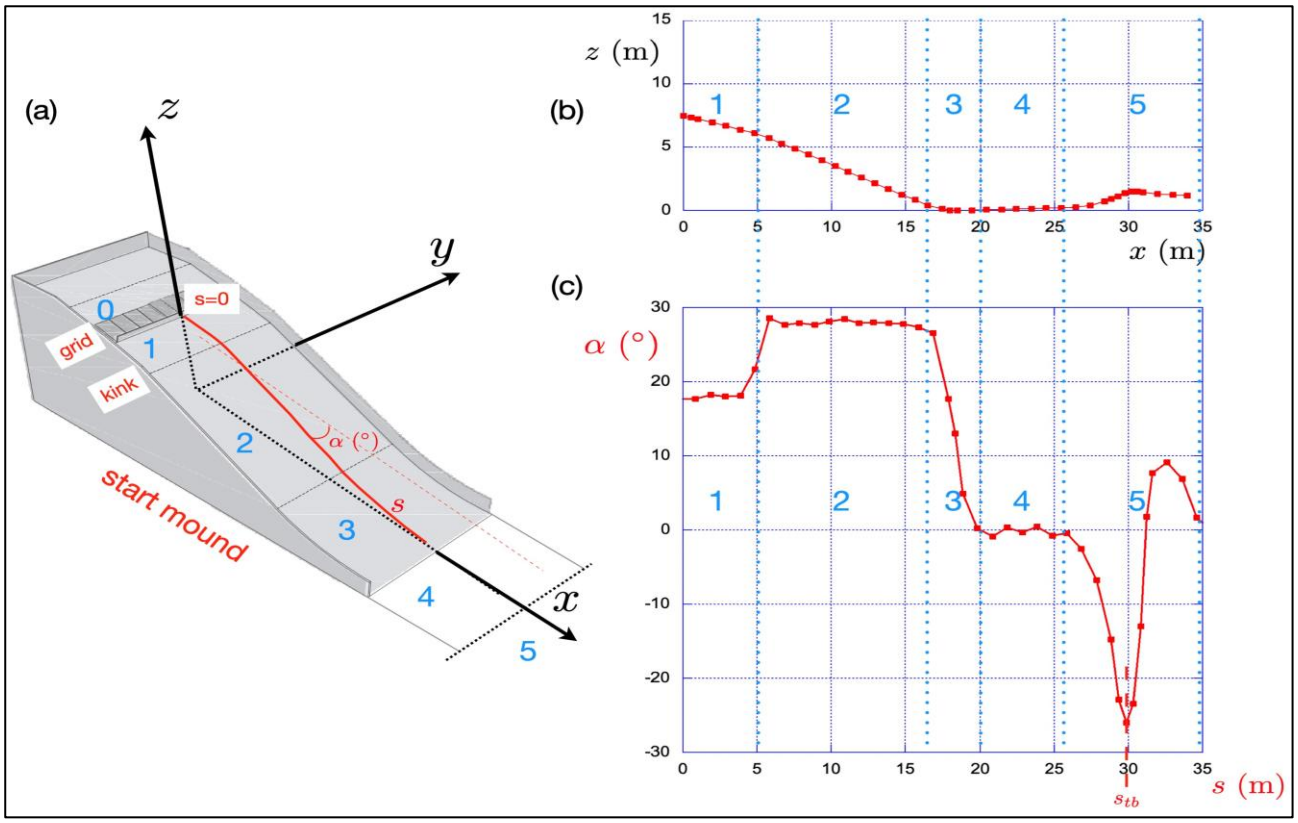

Figure 3. BMX start ramp. (a) 3-D schematic with definition of curvilinear abscissa s and slope $\alpha(s)$; (b) measured side profile at SQY; (c) slope distribution $\alpha(s)$, positive for downhill. Zones 0–5 highlighted in blue correspond to distinct dynamical regimes discussed in the text.

2.2 Pilot and Bike

The rider (age 29; height 1.78 m; mass 80.6 kg) is a member of the French national BMX team, the 2025 world champion, the 2023 world silver medallist, and a two-time European champion (2021 and 2024). His performance characteristics are typical of elite BMX athletes. He uses an Inspyre Concorde V2 frame with 24.7cm wheel radius ($2\pi R$ = 1.55m), tyres inflated to 8 bar. Two gear ratios are employed in training (G = 47/18) and competition (G = 47/17), with an additional G = 47/16 tested for comparison. Protective equipment complies with UCI regulations [3].

The study complied with the Declaration of Helsinki. All data were gathered during the athlete's routine training sessions; no additional intervention was introduced.

2.3 Sensors and Data Acquisition

2.3.1 Force Measurement Via Strain Gauges

A UCI-approved instrumented crankset (Phyling, France) records left and right crank forces at 200Hz [3]. Calibration follows the static-load protocol of Wooles [25]. Normal forces F_{nl} and F_{nr} yield the instantaneous crank torque $\Gamma_{i(t)} = (F_{nl} + F_{nr})\ell_m$ where ℓ_m is crank length (0.175m) (figure 4d).

2.3.2 Cadence and Wheel Speed

Crank angular velocity $\dot{\theta}(t)$ is measured by a tri-axial gyroscope, and wheel speed is inferred from $\dot{\theta}$ using $V = RG\dot{\theta}$.

2.3.3 Instantaneous Power

Power is computed as $P_i(t) = \Gamma_i(t)\,\dot{\theta}(t)$. Cycle-averaged power $P(t)$ is obtained by integration over the pedalling period T.

2.3.4 Data Storage

All channels are logged on a 32GB SD card embedded in the crankset housing, enabling full-session recording for off-line analysis.

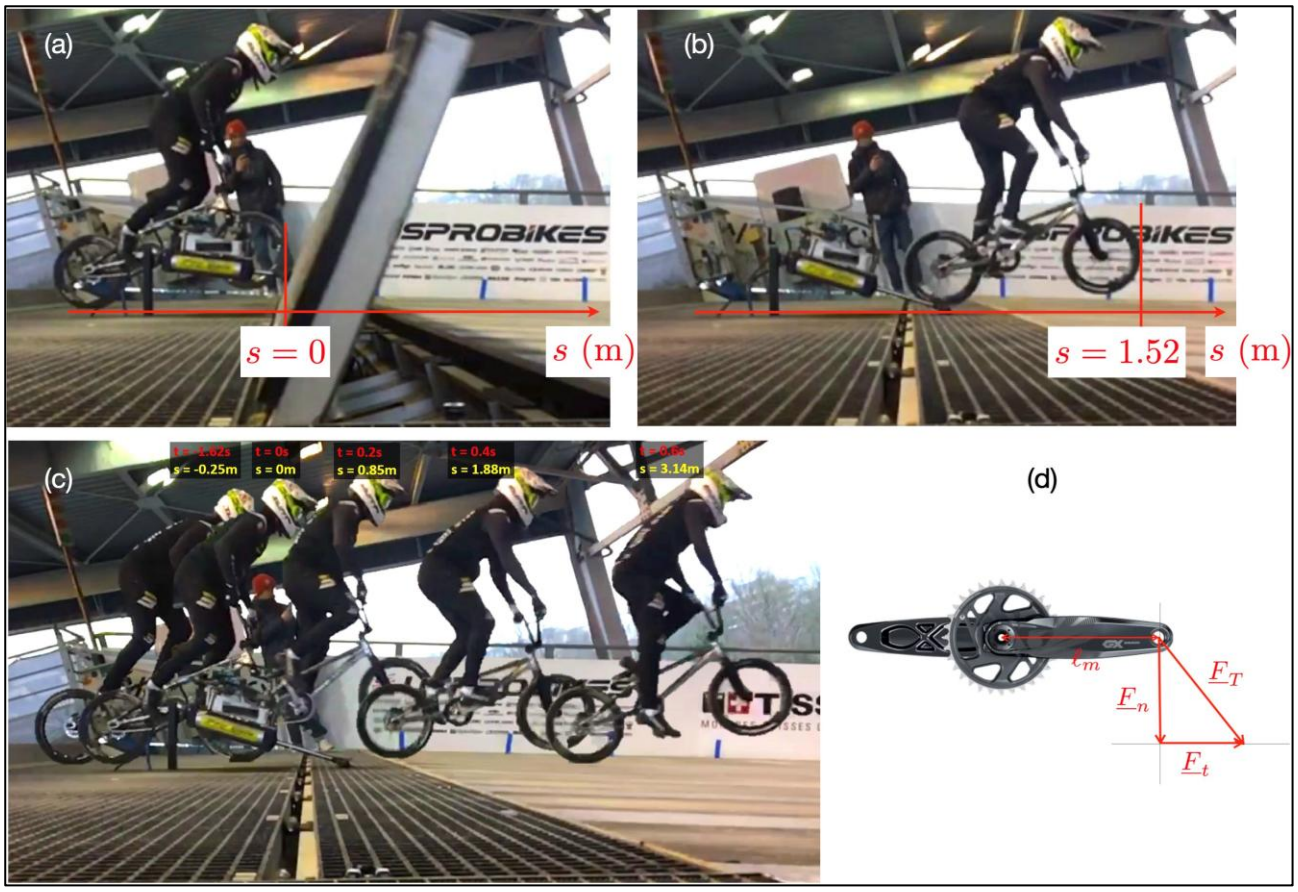

Figure 4. (a) Initial position at $t = 0$, $s = 0$. (b) Position at $t = 0.325$s, $s = 1.52$m. (c) Chronophotograph composed of five frames spaced by 0.20s ($G = 47/17$). (d) Decomposition of forces acting on one crank.

2.4 Protocol

Two sessions employing identical procedures were run five weeks apart. In each session the rider completed five maximal standing starts for each gear ratio. Ambient air density ϱ and free-stream wind velocity v_w were recorded prior to every run. Session 1 ($\rho = 1.21$kgm^{-3}, $v_w = 0.10$m/s) tested $G = 47/17$ and $G = 47/18$; Session 2 ($\rho = 1.18$kgm^{-3}, $v_w = 0.05$m/s) tested $G = 47/17$ and $G = 47/16$. The resulting data sets form the basis for the analyses reported in Sections 3–4.

3 Experimental Results

3.1 Chronophotography of Standing Start

3.1.1 Side View

Figure 4c superimposes five side images acquired 0.20s apart. The origin of time ($t = 0$) corresponds to the green light, and the spatial origin ($s = 0$) is located at the starting gate. During the first 0.20s, the rider covers 0.40m (2m/s); during the last 0.20s, the displacement is 1.8m (9m/s). The average acceleration is therefore

$$\bar{a} = \frac{\Delta V}{\Delta t} = \frac{9 - 2}{0.6} \approx 12\,\mathrm{m\,s^{-2}}\ (\approx 1.2\,g)$$

3.1.2 Front View

Figure 5 combines five front images taken 0.50 s apart. At the end of the ramp the speed is about 15m/s. In the curved transition (Zone 3, $d\alpha/ds \approx 0.20$m^{-1}, $R_c \approx 5$m) the rider experiences a centrifugal acceleration $V^2\,d\alpha/ds \approx 50$ms^{-2}, i.e. approximately $5g$. This five-fold increase in effective weight prevents any pedalling; the athlete therefore freezes on the pedals to absorb the load.

3.2 Quantitative Measures of a BMX Standing Start

3.2.1 *Position, Speed and Forces*

Figure 6a shows the time histories of position $s(t)$ (red) and speed $V(t)$ (blue) over the first 2.2s for the run illustrated in figure 5. The kink (the transition point between Zones 1 and 2) is crossed at t = 1.0s ($V \approx 30\ km/h$) and the bottom of the ramp at t = 2.0s, where the velocity reaches 50 kmh^{-1}.

The mean acceleration on the descent is therefore

$$\bar{a} = \frac{\Delta V}{\Delta t} = \frac{13.9 - 8.3}{1} \approx 5.6\ ms^{-2} (\approx 0.57\ g)$$

exceeding the downhill component of gravity $g \sin\alpha \approx 4.6 ms^{-2}$.

Figure 6b presents the left (F_{nl}) and right (F_{nr}) normal crank forces. Exactly four crank revolutions (N = 4) occur on the start ramp; the peak force drops from 2700N to 800N as cadence rises, consistent with the torque–cadence relationship (see section 5). In the 5g transition area (zone 3) the forces become symmetrical and reach a peak-to-peak value of 3800N, matching $5M_cg$ for the mass of the rider M_c = 80.6kg.

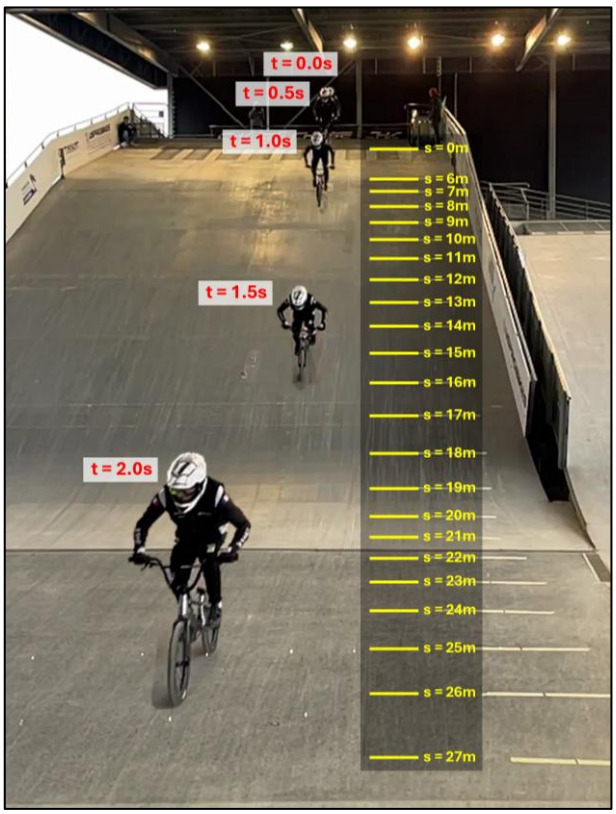

Figure 5. Front chronophotograph of a BMX standing start (G = 47/17). Five frames are spaced by 0.50 s.

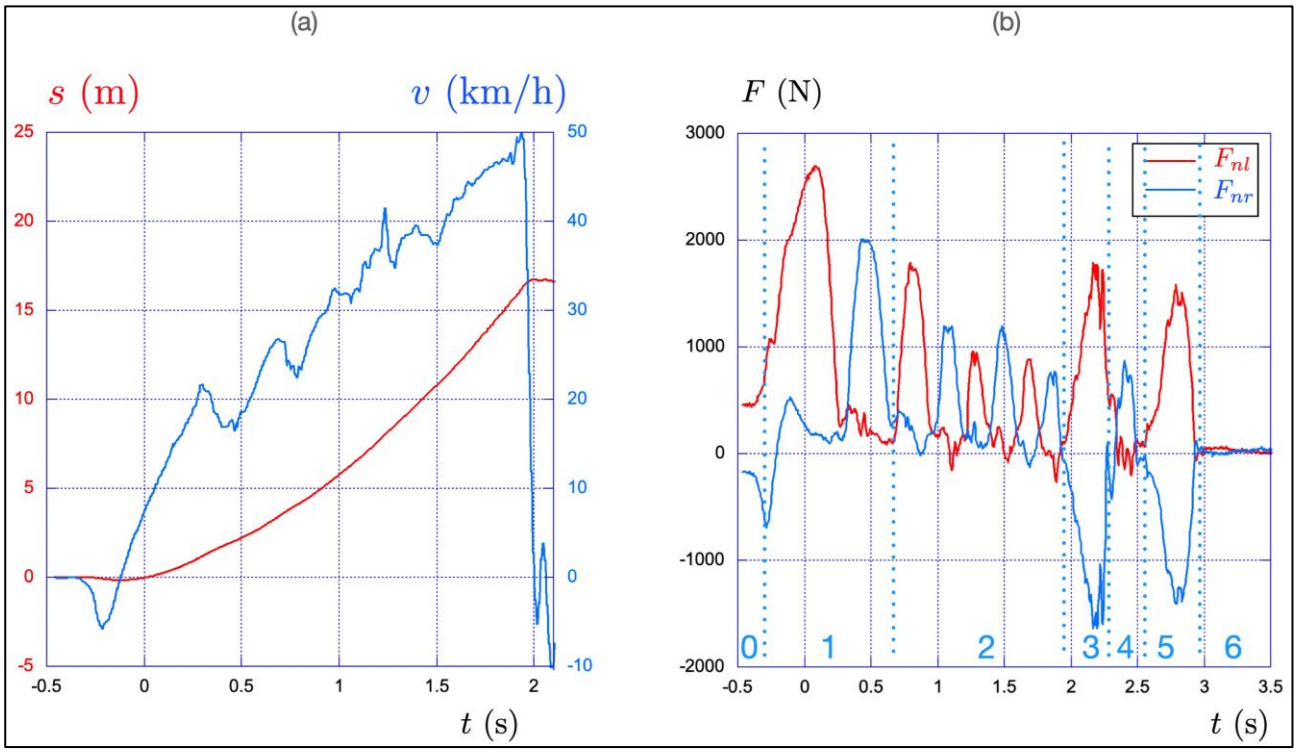

Figure 6. (a) Position $s(t)$ (red) and speed $V(t)$ (blue) during the first 2.2s. (b) Left (F_{nl}, red) and right (F_{nr}, blue) normal forces over 3.5s. The corresponding ramp zones (figure 3) are indicated in blue above the time axis

3.2.2 *Energy and Power*

The instantaneous power $P_i(t) = (Fnl + Fnr)\ell m\,\dot{\theta}$ and its time integral $E(t)$ are shown in figure 7. Eight power peaks between 2400–3700W correspond to the alternate contributions of the two legs during the four crank cycles. Pedalling stops at t = 1.9s (start of Zone 3), reducing power to zero. The cumulative energy reaches 4.0kJ, giving a mean power of 2.1kW; the total energetic cost up to the first bump is 4.4kJ.

3.2.3 *Impact of the Gear Ratio*

Three gear ratios were evaluated: G_1 = 47/16, G_2 = 47/17 and G_3 = 47/18. Figure 8a shows that a larger G produces lower initial acceleration but a longer pedalling distance since the rider performs the same N = 4 revolutions: $2\pi RGN \approx$ 18.2m, 17.1m and 16.1m for G_1, G_2 and G_3, matching the measurement.

The speed traces in figure 8b reveal the highest exit velocity for the largest gear G_1. Nevertheless, figure 8c indicates that total start energy remains close to 4kJ for all ratios: the longer pedalling duration at high G offsets the lower mean power, so the overall energetic cost is almost invariant.

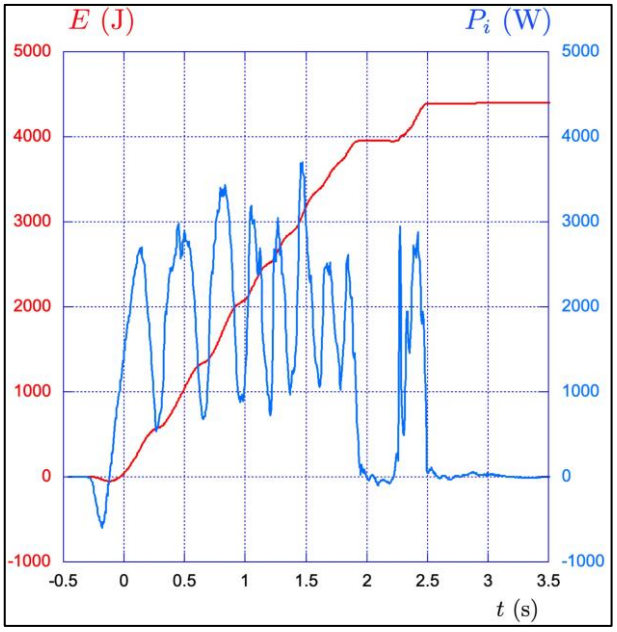

Figure 7. Instantaneous power P_i (blue) and cumulative energy E (red) over the first 4s for the run shown in figure 6.

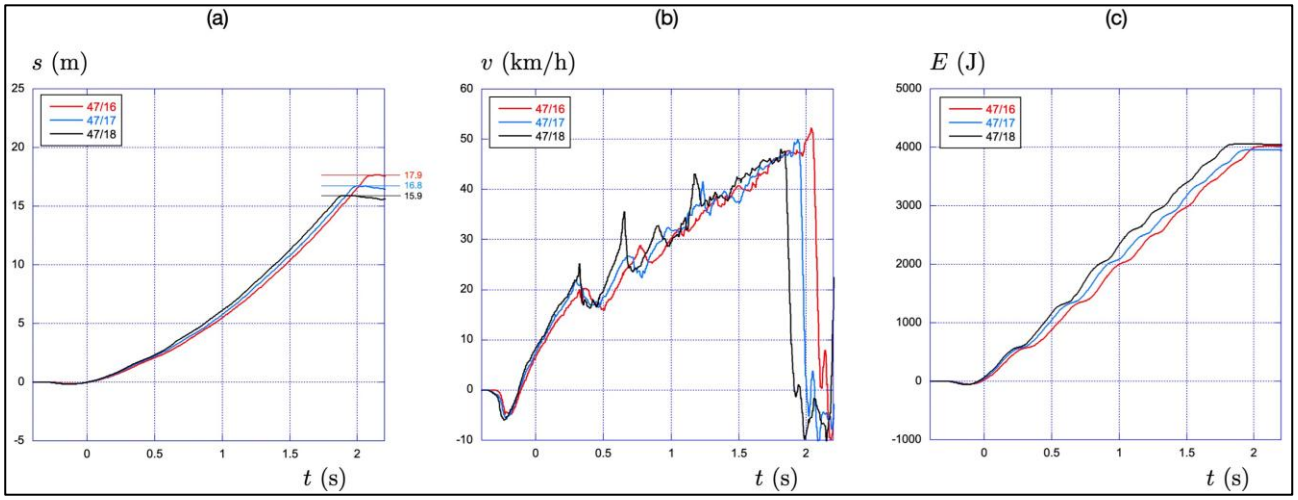

Figure 8. Influence of gear ratio: (a) trajectory $s(t)$, (b) speed $V(t)$ and (c) cumulative energy $E(t)$ for G_1 = 47/16, G_2 = 47/17 and G_3 = 47/18.

4 Physical Model

4.1 Energy Balance

The mechanical energy of the rider–bicycle system consists of translational kinetic energy and gravitational potential energy,

$$\frac{1}{2}MV_G^2 + Mgz_G$$

where $M = M_c + M_b$ is the combined mass of rider (M_c = 80.6kg) and bicycle (M_b = 9kg), V_G the speed of the centre of mass, z_G its vertical position, and g = 9.81ms^{-2}.

The temporal evolution of this energy is governed by the muscular power delivered by

the rider, P, reduced by the drivetrain efficiency $\eta < 1$, and by the power dissipated through aerodynamic drag and rolling resistance, P_f:

$$\frac{d}{dt}\left(\tfrac{1}{2}MV_G^2 + Mgz_G\right) = \eta P - P_f$$

Equation (1)

In all calculations we use a constant drivetrain efficiency $\eta = 0.92$, representative of a BMX drivetrain.

Following wind-tunnel and drum-bench measurements (Appendices A–B), the loss term is modelled a

$$P_f = \tfrac{1}{2}\rho\, SC_D\, V_G^3 + C_{RR}\, M g\, V_G \cos\alpha$$

with ρ the air density, $SC_D = 0.55\text{m}^2$ the drag area, $C_{RR} = 0.0093$ the rolling-resistance coefficient, and $\alpha(s)$ the local slope of the ramp (figure 3c).

Because α is known as a function of arc length s but not as a function of time, we rewrite Equation 1 in curvilinear coordinates using $ds = V_G\, dt$ and $dz_G/ds = -\sin\alpha$:

$$\frac{dV_G^3}{ds} = \frac{3\eta P}{M} + 3g\, V_G \sin\alpha(s) - \frac{3\rho SC_D}{2M}\, V_G^3 - 3C_{RR}\, g\, V_G \cos\alpha(s)$$

Equation (2)

Equation (2) predicts the speed profile along the start ramp once the rider's power output $P(s)$ is specified.

4.2 Validation of the Physical Model

The model is validated against the instrumented-crank and gyroscope data introduced in Section 3. For each half-crank cycle we compute the average power P and integrate Equation (2) numerically (explicit Euler scheme) using the measured initial conditions. Figure 9a illustrates both the instantaneous power P_i and the corresponding half-cycle average P for a representative run with $G = 47/17$.

The resulting speed prediction (red squares in figure 9b) closely follows the velocity measured with the gyroscope (black squares) throughout the ramp. For completeness, the figure also shows the prediction of the fully coupled model—including the biomechanical power law introduced in Section 5—given by Equation (3) (solid blue line). The excellent agreement supports the suitability of Equation (2) as a dynamical description of BMX start mechanics, provided that the rider's instantaneous power is known.

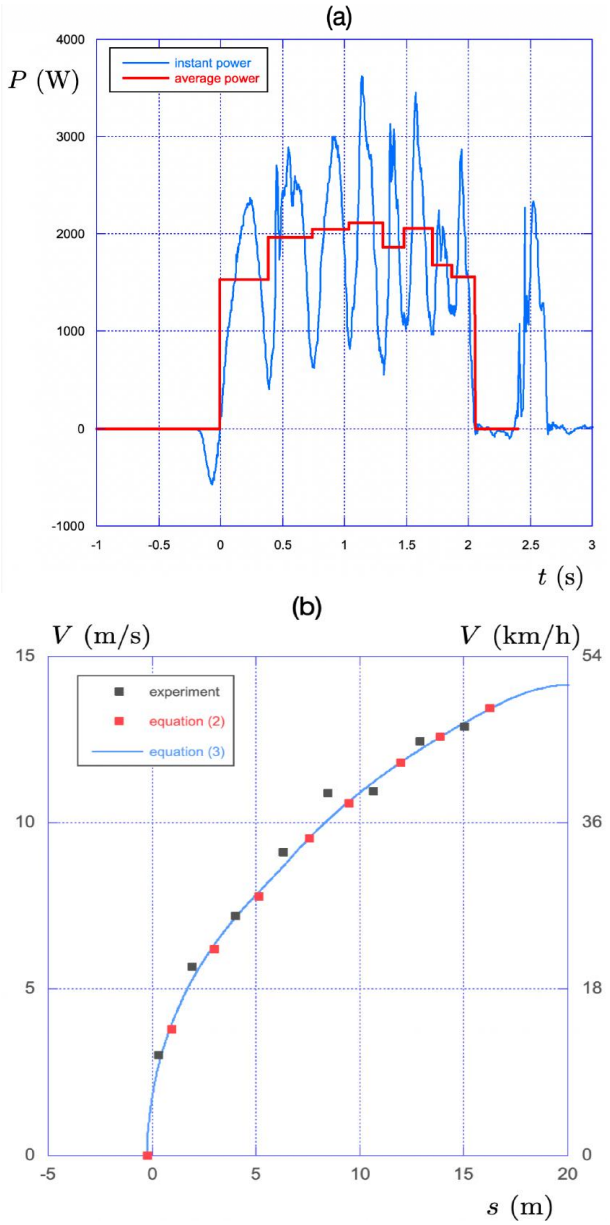

Figure 9. (a) Instantaneous mechanical power P_i (blue) and average power per half crank cycle P (red) for a start with $G = 47/17$. (b) Velocity measured with the on-board gyroscope (black squares) compared with the prediction obtained from Equation (2) using measured average power (red squares) and with the complete model Equation (3) (solid blue line).

5 The Biomechanical Model for the Injected Power, *P*

Bobbert [26] showed that the force–velocity relationship of a multi-articulated human limb system is quasi-linear. In cycling this translates into an approximately linear link between the crank torque Γ and the pedalling rate $\dot{\theta}$ [27, 28, 29, 30, 31].

The instantaneous mechanical torque is

$$\Gamma_i(t) = \left(F_{nl}(t) + F_{nr}(t)\right)\ell_m$$

Here we use its cycle-average value

$$\Gamma(t) = \frac{1}{T}\int_t^{t+T} \Gamma_i(t')\,dt'$$

with *T* the duration of one crank revolution.

Figure 10 pools data from multiple standing starts performed with *G* = 47/17 and *G* = 47/18.

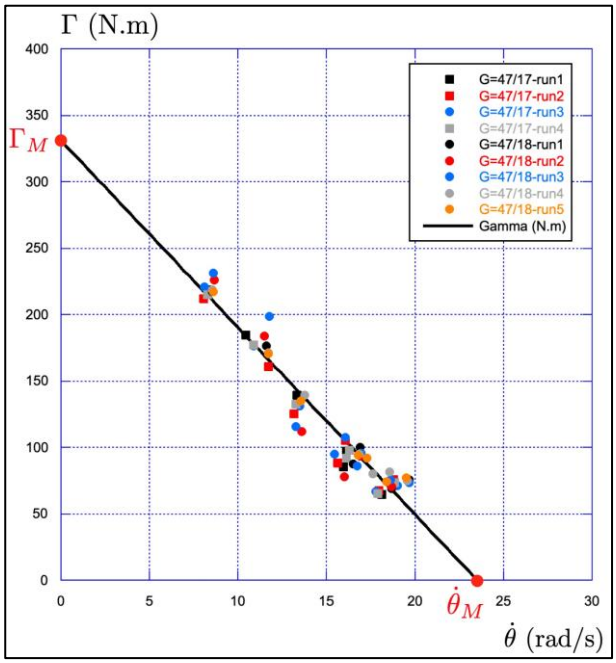

Figure 10. Mean crank torque Γ versus pedalling rate $\dot{\theta}$ for several standing starts using gear ratios *G* = 47/17 and *G* = 47/18.

A linear regression yields

$$\Gamma = \Gamma_M\left(1 - \frac{\dot{\theta}}{\dot{\theta}_M}\right)$$

where the maximal (zero-cadence) torque and maximal cadence are Γ_M = 331Nm and $\dot{\theta}_M$ = 23.5rads^{-1}, respectively.

The solid line is the linear regression $\Gamma = \Gamma_M\left(1 - \frac{\dot{\theta}}{\dot{\theta}_M}\right)$.

Using the above linear law, the average muscular power becomes

$$P = \Gamma\,\dot{\theta} = \Gamma_M\left(1 - \frac{\dot{\theta}}{\dot{\theta}_M}\right)\dot{\theta}$$

Because the rider freewheels only after leaving the ramp, cadence and bicycle speed are linked by

$$V_G = RG\,\dot{\theta}$$

with *R* the wheel radius and *G* the gear ratio. Substituting $\dot{\theta} = V_G/(RG)$ gives

$$P = \Gamma_M\left(1 - \frac{V_G}{RG\dot{\theta}_M}\right)\frac{V_G}{RG}$$

Inserting this expression into the energy balance G (2) yields the fully coupled, non-linear differential equation governing the speed evolution along the ramp:

$$\frac{dV_G^2}{ds} = \frac{2\eta\Gamma_M}{MRG}\left(1 - \frac{V_G}{RG\dot{\theta}_M}\right) + 2g\sin\alpha(s) - \left(\frac{\rho S C_D}{M}V_G^2 + 2C_{RR}g\cos\alpha(s)\right)$$

Equation (3)

The only free parameter in Equation (3) is the gear ratio *G*, making it a convenient tool for start performance optimisation.

6 Various Optimisations

6.1 The maximum Gear Ratio G_{max}

The rider involved in the present study always completes exactly four crank revolutions on the ramp before entering Zone 3, where the ~5*g* load prevents pedalling. With a maximum pedalling distance of $d_{max} \approx$ 18m to the start of Zone 3 (figure 3), the kinematic constraint

$$4\left(2\pi RG\right) \le d_{\max}$$

imposes an upper bound

$$G_{\max} = \frac{d_{\max}}{8\pi R} \simeq 2.90$$

corresponding to the practical choice 47/16.

6.2 Minimising the Start Time T_s

A first optimisation goal is to minimise the time required to travel from the gate (s = 0) to the crest of the first bump ($s = s_{tb}$ in figure 3c). We numerically integrate Equation (3) for admissible gear ratios and compute the resulting start time $T_s(G)$. Figure 11a reveals a shallow optimum at $G_{opt} = 2.802$ (close to 45/16). Relative to the competitor's current ratio 47/17 the benefit is negligible—about 0.03ms, i.e. 0.4mm at 50kmh^{-1} and thus of little practical value.

6.3 Maximising Mean Acceleration on the Ramp

Discussions with the coach highlighted that entering the flat section (Zone 4) with higher speed is tactically preferable, even at the cost of a slight delay at the top of the bump. We therefore defined an alternative criterion: maximise the average acceleration between s = 6m (exit of the kink) and s = 18m (start of Zone 3),

$$\bar{\gamma} = \frac{V(s = 18) - V(s = 6)}{t(s = 18) - t(s = 6)}$$

Figure 11b shows that this criterion is maximised by the largest permissible gear, G_{max} = 2.90. Hence the competition ratio 47/17 already outperforms the training ratio 47/18, and a modest increase towards 47/16 could further enhance acceleration without violating the four-revolutions constraint.

A compromise that balances both criteria (T_s and $\bar{\gamma}$) is obtained around G = 2.85 (e.g. 37/13).

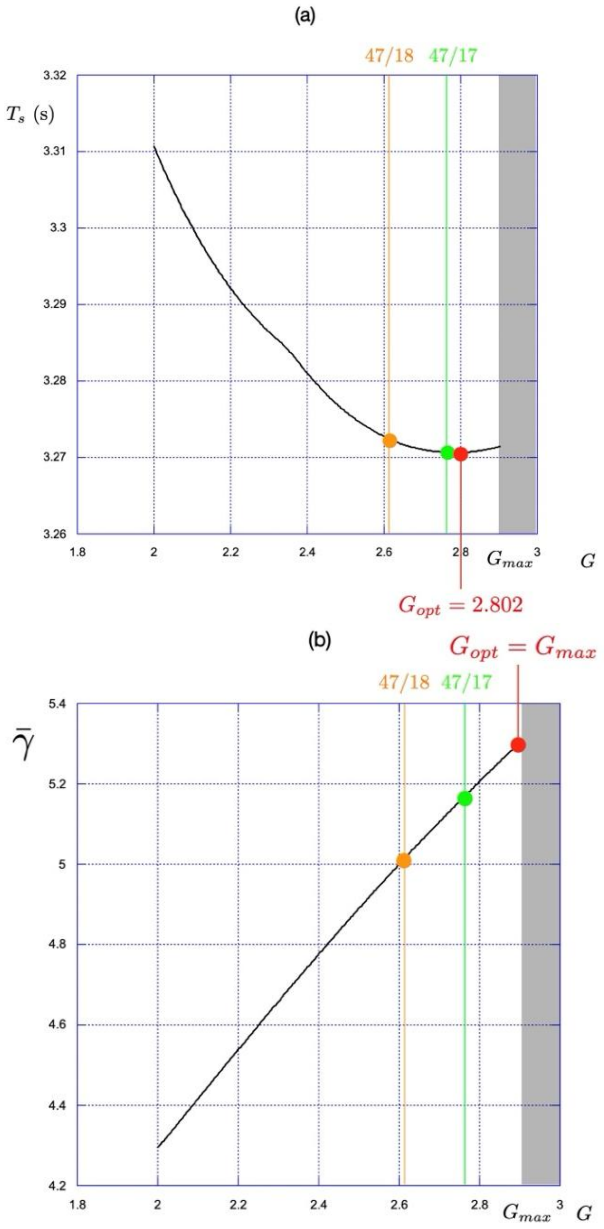

Figure 11. (a) Start time T_s from gate to bump versus gear ratio G. (b) Mean acceleration $\bar{\gamma}$ between s = 6m and s = 18m versus G. Dashed lines indicate the tested ratios 47/18, 47/17 and the upper limit 47/16.

7 Conclusions and Perspectives

Using high-frequency on-track measurements, we established and validated a physics-based model that couples the topography of an Olympic BMX start ramp with the rider's individual torque–cadence capability. The formulation predicts the velocity profile over the first ↑30 m of the race and requires only readily measurable inputs: crank torque, cadence and ramp geometry.

When the model is combined with simple performance criteria, it becomes a practical decision aid for coaches. For the elite rider studied here, minimising the time to the first bump yields an optimal gear ratio $G_{opt} = 2.802$ (≈ 45/16), yet the time advantage over the current competition ratio 47/17 is negligible. Conversely, maximising the mean acceleration between the kink and the flat favours the largest admissible ratio ($G_{max} = 2.90$; 47/16), providing a tangible speed benefit at the ramp exit. The choice of objective therefore has a non-trivial influence on gearing strategy and should be aligned with tactical goals agreed upon by rider and coach.

Two limitations merit future work. First, the present analysis is restricted to the start phase (first 3s) whereas BMX races last roughly 35–40s. Extending the model to the entire track—either by segmenting later sections or by embedding a fatigue component—would enable a whole-race optimisation. Second, all data were collected in solo runs; interactions with opponents, aerodynamic shielding and strategic line changes remain unexplored. Controlled multi-rider experiments and computational fluid-dynamics coupling would help address these aspects.

Funding: This research received no external funding.

Conflicts of Interest: The authors declare no conflict of interest.

References

[1] Herlihy D.V. *Bicycle: the history*. Yale University Press, 2004.

[2] Steinbach A.B. Social facilitation in bmx racing. *Halle: Faculty of Sports Sciences of the Martin Luther-Universitat Halle-Wittenberg, University of Halle*, 2014.

[3] Union Cycliste Internationale. UCI cycling regulations, part VI: BMX racing. https://assets.ctfassets.net/761l7gh5x5an/122Ylx2XJjbqzh6xPCu7sK/1bf2d669421b125e5c8c9a5262799904/20221205_-6-BMX-ENG-left_column_final.pdf, 2023. Official regulations defining minimum dimensions and standards; consulted 2023 edition.

[4] Wade N. The historical mediatization of BMX-freestyle cycling. *Sport in Society*, 13(7-8):1152– 1169, 2010.

[5] Koellner A., Cameron C.J., and Battley M.A. Structural responses on a BMX racing bicycle. *Procedia Engineering*, 72:618–623, 2014. The Engineering of Sport 10.

[6] Bertucci W., Hourde C., Manolova A., and Vettoretti F. Facteurs mécaniques de la performance lors de la phase d'accélération en BMX chez des pilotes entraînés. *Science & Sports*, 22(3):179–181, 2007.

[7] Debraux P. and Bertucci W. Determining factors of the sprint performance in high-level BMX riders. *Computer Methods in Biomechanics and Biomedical Engineering*, 14(sup1):53–55, 2011.

[8] Bertucci W. and Hourde C. Laboratory testing and field performance in BMX riders. *J Sports Sci Med*, 10(2):417–419, 2011.

[9] Debraux P., Manolova A.V., Soudain-Pineau M., Hourde C., and Bertucci W. Maximal torque and power pedaling rate relationships for high level BMX riders in field tests. *Journal of Science and Cycling*, 2:51–57, 2013.

[10] Cowell J.F., Cronin J.B., and McGuigan M.R. Time motion analysis of supercross BMX racing. *J Sports Sci Med*, 10(2):420–421, 2011.

[11] Cowell J.F., McGuigan M.R., and Cronin J.B. Movement and skill analysis of supercross bicycle motocross. *The Journal of Strength & Conditioning Research*, 26(6), 2012.

[12] Zabala M., Requena B., Sanchez-Munoz C., Gonz´alez-Badillo J.J., Garcıa I., Oopik V., and Paasuke M. Effects of sodium bicarbonate ingestion on performance and perceptual responses in a laboratory-simulated BMX cycling qualification series. *The Journal of Strength & Conditioning Research*, 22(5):1645–1653, 2008.

[13] Maw S., Proctor L., Vredenburg J., and Ehlers P. Influence of starting position on finishing position in world cup 500 m short track speed skating. *Journal of Sports Sciences*, 24(12):1239– 1246, 2006.

[14] Pilianidis T., Kasabalis A., Mantzouranis N., and Mavvidis A. Start reaction time and performance at the sprint events in the olympic games. *Kinesiology*, 44(1):67–72, 2012.

[15] Rylands L. and Roberts S.J. Relationship between starting and finishing position in world cup BMX racing. *International Journal of Performance Analysis in Sport*, 14(1):14–23, 2014.

[16] Grigg J., Haakonssen E., Orr R., and Keogh J.W. Literature review: Kinematics of the BMX gate start. *Journal of Science and Cycling*, 6(1):3–10, Jun. 2017.

[17] Di Rienzo F., Martinent G., Levêque L., MacIntyre T., Collet C., and Guillot A. The influence of gate start position on physical performance and anxiety perception in expert BMX athletes. *Journal of Sports Sciences*, 36(3):311–318, 2018.

[18] Princelle D. *Analyse biomécanique multi corps et évaluation de la performance lors du départ en BMX race*. Theses, Université de Poitiers, May 2021.

[19] Mateo-March M., Fernandez-Pena E., Blasco-Lafarga C., Morente-S´anchez J., and Zabala M. Does a non-circular chainring improve performance in the bicycle motocross cycling start sprint ? *J Sports Sci Med.*, 13(1):97–104, 2014.

[20] Mateo M., Blasco-Lafarga C., and Zabala M. Pedaling power and speed production vs. technical factors and track difficulty in bicycle motocross cycling. *The Journal of Strength & Conditioning Research*, 25(12), 2011.

[21] Zabala M., Sanchez-Munoz C., and Mateo M. Effects of the administration of feedback on performance of the BMX cycling gate start. *Journal of Sports Science and Medicine*, 8:393–400, 2009.

[22] Grigg J., Haakonssen E., Rathbone E., Orr R., and Keogh J.W.L. The validity and intra-tester reliability of markerless motion capture to analyse kinematics of the BMX supercross gate start. *Sports Biomechanics*, 17(3):383–401, 07 2018.

[23] Elvira J.L.L., Mateo-March M., Zabala M., and Blasco-Lafarga C. The use of accelerometry to evaluate the BMX cycling starting hill. effect of the q-ring on the acceleration profile. *Sports Biomechanics*, 22(7):906–920, 07 2023.

[24] Union Cycliste Internationale. UCI BMX track guide. https://assets.ctfassets.net/761l7gh5x5an/3bfMtEa6B9acxJjLjp53EU/c126181d241519b0d055365fe4867755/uci-bmx-track-guide-2017-v-final.pdf, 2017. Guidelines on BMX track and start hill geometry for UCI-sanctioned events.

[25] Wooles A.L., Robinson A.J., and Keen P.S. A static method for obtaining a calibration factor for srm bicycle power cranks. *Sports Engineering*, 8(3):137–144, 2005.

[26] Bobbert M.F. Why is the force-velocity relationship in leg press tasks quasi-linear rather than hyperbolic? *Journal of Applied Physiology*, 112(12):1975–1983, 2012.

[27] Sargeant A.J., Hoinville E., and Young A. Maximum leg force and power output during short-term dynamic exercise. *J Appl Physiol: Respirat Environ Exercise Physiol*, 51:1175–1182, 1981.

[28] McCartney N., Heigenhauser G.J., and Jones N.L. Power output and fatigue of human muscle in maximal cycling exercise. *Journal of Applied Physiology: Respiratory, Environmental and Exercise Physiology*, 55(1):218–224, 1983.

[29] Vandewalle H., Peres G., Heller J., Panel J., and Monod H. Force-velocity relationship and maximal power on a cycle ergometer. *Eur J Appl Physiol*, 56:650–656, 1987.

[30] Dorel S., Hautier C.A., Rambaud O., Rou"et D., Van Praagh E., Lacour J.R., and Bourdin M. Torque and power-velocity relationships in cycling: Relevance to track sprint performance in world-class cyclists. *Int J Sports Med*, 26:739–746, 2005.

[31] Rivière J.R., Peyrot N., Cross M., Messonnier L., and Samozino P. Strength-endurance: Interaction between force-velocity condition and power output. *Frontiers in Physiology*, 11:1237, 2020.

Appendix A. Measurements of the Drad Area SC_D

The aerodynamic drag area SC_D was determined in a Gustave-Eiffel type wind tunnel. The BMX bicycle was rigidly mounted on a six-component force balance (figure A1a); the rider adopted the *standing* posture used on the start ramp (figure A1b). For each test, air speed was increased stepwise to 15m/s and the steady-state drag force F_D recorded. The drag area follows from $F_D = \frac{1}{2}\rho SC_D U^2$, with ρ the tunnel air density and U the flow speed.

Across six repeats the mean value was

$$SC_D = 0.50 \pm 0.05 \text{ m}^2$$

Because winter clothing worn during the field campaign increases frontal area, we employ the conservative upper-bound $SC_D = 0.55\text{m}^2$ in the modelling sections.

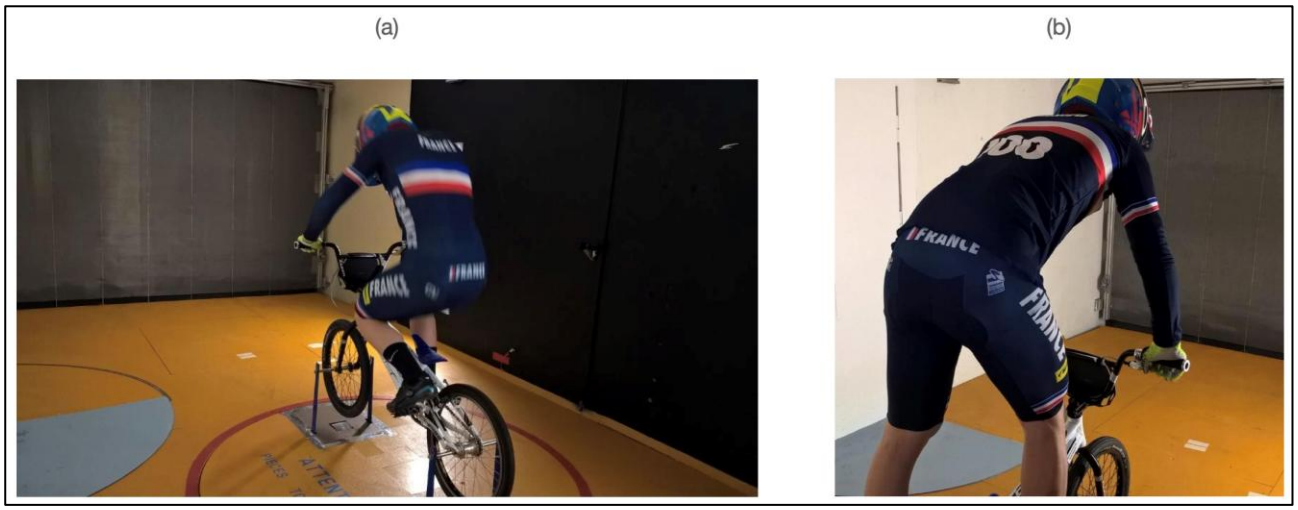

Figure A1. Wind-tunnel set-up for aerodynamic drag measurement. (a) Rider seated for calibration; (b) standing position used on the start ramp, retained for SC_D estimation.

Appendix B. Measurements of the Rolling-Resistance Coefficient C_{RR}

Rolling resistance was quantified on a motor-driven drum bench (figure B1a). A wooden drum of radius $R_W = 0.5$ m rotates at a tangential speed of 50 km/h . Torque is recorded by an in-line transducer in three stages (figure B1b):

(i) *Drum only*: baseline torque Γ_0.

(ii) *Unloaded contact*: bicycle wheel in contact without additional normal load, torque Γ_1.

(iii) *Loaded contact*: vertical load Mg applied to the hub, torque Γ_2.

The increase $\Delta\Gamma = \Gamma_2 - \Gamma_1$ corresponds to the moment due to rolling resistance. The coefficient is obtained from

$$C_{RR} = \frac{\Delta\Gamma}{MgR_W}$$

With a tyre pressure of 8 bar the mean value was

$$C_{RR} = 0.0093$$

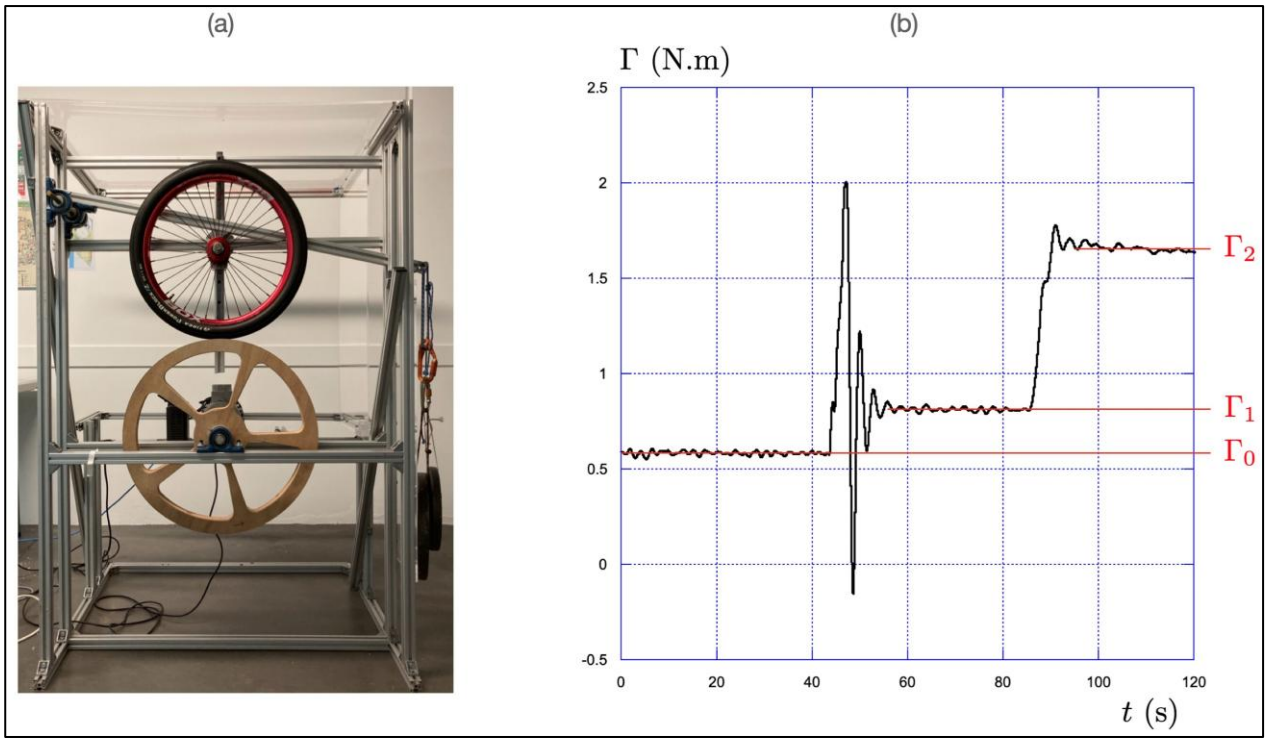

Figure B1. Rolling-resistance measurement. (a) Drum bench with torque transducer; (b) example torque trace showing the three measurement phases.